SIN-CHN
SCIENTIFIC PRESS PTE.LTD.

Molecular & Cellular Biomechanics 2024, 21(3), 414.
https://doi.org/10.62617/mcb414

Article

Magnetic resonance imaging diagnosis of ankle joint athletic injury based on machine learning algorithms

Hongxia Han[1], Yuanwei Li[2,*]

[1] Department of Physical Education and Research, Harbin Finance University, Harbin 150030, Heilongjiang, China
[2] Department of basic courses, Wuhan Qingchuan University, Wuhan 430204, Hubei, China
*** Corresponding author:** Yuanwei Li, liyuanwei1011@163.com

CITATION

Han H, Li Y. Magnetic resonance imaging diagnosis of ankle joint athletic injury based on machine learning algorithms. Molecular & Cellular Biomechanics. 2024; 21(3): 414.
https://doi.org/10.62617/mcb414

ARTICLE INFO

Received: 24 September 2024
Accepted: 8 October 2024
Available online: 8 November 2024

Abstract: The diagnosis of ankle joint athletic injuries using traditional magnetic resonance imaging (MRI) relies on the subjective judgment and experience of doctors, and small structural changes in athletic injuries are difficult to accurately detect and diagnose. By using machine learning (ML) algorithms and image processing techniques to obtain objective and consistent diagnostic results, the accuracy of diagnosing ankle joint athletic injuries can be improved. This article collected a large number of MRI images of ankle joint athletic injuries, and preprocessed the collected images to extract morphological and texture features, and perform feature fusion. The Residual Network (ResNet) was improved, and the Leaky linear rectification function (ReLU, Corrected linear unit) activation function was introduced. The transfer learning was utilized to increase the convergence speed of the model, and the global maximum pooling layer and softmax classifier were used to construct the fully connected layer. After sufficient training on the training set, the findings on the test set indicated that the average accuracy of the improved ResNet model for ankle joint injury classification was 98.3%. The use of an improved ResNet model can effectively improve the diagnostic effectiveness of ankle joint athletic injuries, providing a new method for medical diagnosis of MRI.

Keywords: magnetic resonance imaging; ankle joint athletic injury; imaging diagnosis; machine learning; improved residual network

1. Introduction

Many popular sports require athletes to engage in intense confrontational running, and the ankle joint is responsible for supporting weight, balance, and executing movements in the human body. In sports such as football, basketball, and rugby, the intensity of exercise is very intense. Ankle joint injury is one of the common athletic injuries, which involves injuries to ligaments, muscles, bones, or other soft tissue structures in the ankle joint [1,2]. Ankle joint injury can cause severe pain, swelling, and other symptoms, and can reduce athletes' exercise level, which has a negative impact on patients' mental health. MRI can display detailed information on soft tissue structure and bones, and doctors can detect tears or strains of ligaments, inflammation of muscles or tendons, and other abnormalities in soft tissue through MRI [3,4]. However, the information obtained by doctors from MRI is mostly based on experience, which may lead to incomplete diagnosis of ankle joint athletic injury [5,6]. In order to provide a more objective and accurate interpretation of imaging information, ML algorithms are used for automated MRI diagnosis, which can reduce the misdiagnosis rate of ankle joint athletic injury and ensure that patients can receive the correct treatment and rehabilitation plan as soon as possible.

Ankle joint is one of the most stressed joints in sports activities, and ankle joint injuries can cause significant injuries to athletes. Many people use MRI to display detailed information about the ankle joint for diagnosing athletic injuries. MRI can clearly display the skeletal structure, surrounding ligaments, muscles, neural structures, etc., of the ankle joint. Through high-resolution ankle joint images, doctors can evaluate the structure and health status of the ankle joint in detail, thereby helping to diagnose injuries or diseases and develop treatment plans [7,8]. In order to comprehensively diagnose injuries to the ankle and foot, Gorbachova Tetyana diagnosed common traumatic and degenerative tendon pathology, abnormalities in the tarsal and tarsometatarsal joint complexes, pathological conditions affecting the joint capsule structure of the big and small toes, and pedal infections through MRI [9]. Alves Timothy explained ultrasound scanning techniques and evaluated potential defects in ankle joint ligaments, and provided ultrasound findings related to MRI of normal and injured ankle joint ligaments. MRI can be used to diagnose injuries to the lateral complex and medial/deltoid complex [10]. Sawant Yogini Nilkantha's study pointed out that ankle joint injury is a common sprain that affects ligaments. MRI can provide accurate diagnosis and appropriate treatment based on complex anatomical knowledge of ankle joint ligaments and the entire pathological range [11]. In order to accurately evaluate the diagnostic effectiveness of deep deltoid ligament injury, Warner Stephen J compared the ability of none stress and stress X-ray films and MRI to diagnose deep deltoid ligament rupture in surgical treatment of ankle joint fractures [12]. MRI can provide a detailed display of the ankle joint injury area, but traditional MRI diagnosis mainly relies on doctor experience to diagnose the content of MRI images, which cannot achieve automated diagnosis and has problems in detecting small structural changes.

ML can quickly diagnose pathology by learning a large number of medical images, and many people use ML algorithms to assist in medical image diagnosis. By extracting pathological features from medical images, the utilization of ML in medical image diagnosis can effectively improve diagnostic speed and accuracy, and reduce human errors [13,14]. Giger Maryellen L's research pointed out that radiomics is an extension of computer-aided diagnosis, converting images into usable data for pathological diagnosis. The application of ML in radiology has a substantial clinical impact on conventional imaging examinations obtained in clinical practice, providing opportunities for improving decision support in medical image interpretation [15]. Medical images are considered as the actual source of appropriate information required for disease diagnosis. The use of various methods to detect diseases in the initial stage is one of the most important factors in reducing cancer and tumor mortality. Computer assisted detection using deep learning and ML has shown significant growth in the medical field [16,17]. Yadav Samir S applied algorithms based on convolutional neural networks (CNNs) to the chest X-ray dataset for pneumonia classification, effectively improving the application effect of medical image classification in clinical treatment and teaching tasks [18]. Imaging technology is utilized to capture abnormalities in the human body, and the captured images are used for the diagnosis, prognosis, and treatment plan of abnormalities. The use of CNNs can effectively classify, segment, locate, and detect medical images [19,20]. Using ML for medical imaging diagnosis can achieve automated pathological diagnosis, providing doctors

with diagnostic results quickly and accurately. However, there is a lack of application of ML algorithms in MRI for diagnosing ankle joint athletic injuries.

The subjectivity and empiricism of traditional MRI diagnosis in ankle joint athletic injuries limit diagnostic accuracy. Combining ML algorithms with MRI can improve the diagnostic effectiveness of ankle joint athletic injuries. This study required obtaining a large number of MRI images and preprocessing them, including image denoising, image registration, image segmentation, and data standardization, to obtain morphological and texture features of the images. The ResNet model was improved, including modifying ReLU to Leaky ReLU, using transfer learning to initialize model weights, and using a global maximum pooling layer and softmax classifier to replace the fully connected layer. The experimental section compared the improved ResNet model with ResNet-50, Inception, Support Vector Machine (SVM), and Random Forest (RF). The results showed that the improved ResNet model had high stability and could effectively improve the accuracy of ankle joint athletic injury classification.

2. Diagnostic methods for ankle joint athletic injuries

2.1. Collection of MRI image data

Sports have developed rapidly, and the vast majority of sports are inseparable from the use of the ankle. In sports that require quick turns, jumps, runs, or unstable weight support, ankle injuries have become very common. The ankle joint is composed of the tibia, fibula, and tarsal bones, responsible for supporting weight, maintaining balance, and withstanding a large amount of pressure and impact during exercise.

Intense exercise can easily cause ankle joint injuries, and common types of ankle joint injuries include ankle joint sprains, ankle joint ligament injuries, ankle bone fractures, ankle joint tendon injuries, and ankle muscle strains [21,22]. Ankle joint athletic injuries can have a dual impact on athletes' physical and psychological well-being. Symptoms of ankle joint injuries include pain, swelling, congestion, making it difficult for athletes to walk, and even ruining their career [23,24].

MRI and other methods can effectively obtain images of the ankle joint, displaying the details of ligament tears or strains around the ankle joint. Doctors can diagnose ankle joint athletic injuries and develop treatment plans through MRI. ML algorithms can diagnose ankle joint athletic injuries by learning from MRI images. Collecting enough MRI images of ankle joint athletic injury is the foundation for ankle joint diagnosis.

This article selects 1500 patients with ankle joint athletic injuries. The selected patients are selected by clinical doctors based on clinical history and symptoms. All selected ankle joint athletic injury patients meet the applicable conditions for MRI examination, and agree to use MRI images for the diagnosis and analysis of ankle joint athletic injury.

The age range of patients covers a wide range, focusing on the main high-risk groups of sports injuries between the ages of 20 and 50, especially young athletes and middle-aged people. Patients' occupations are mainly divided into three categories: professional athletes, amateur athletes and non-athletes. The frequency and type of sports injuries in professional athletes are significantly different from those in the

general population, so this information can help the model distinguish the risk of injury at different exercise intensities.

Patients need to choose appropriate postures, such as lying flat, sitting, or lying on their abdomen, in order to obtain images from different angles. The 3T MRI system is used to obtain high-resolution images. Patients must obtain clear informed consent and explain the purpose, risks, and benefits of the study before conducting MRI image acquisition. Moreover, after obtaining MRI images, it is necessary to ensure that the patient's privacy is protected and patient identity information is not leaked.

The MRI image acquisition process of ankle joint athletic injury is shown in **Figure 1**.

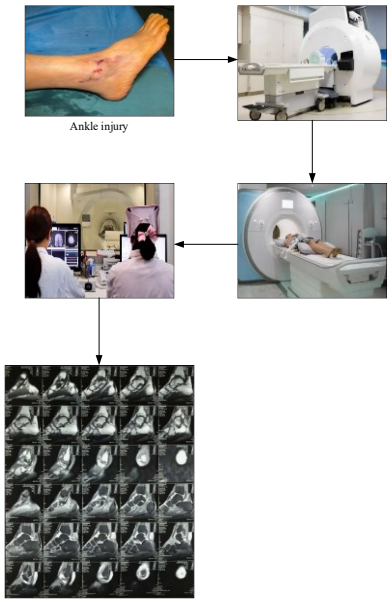

Figure 1. Image acquisition process.

In **Figure 1**, the process of MRI image acquisition is described. Suitable individuals with ankle joint athletic injuries are selected and scanned using MRI machines in specific postures. Medical staff print MRI images of the ankle joint injury area based on the scanning results.

When collecting MRI images, the data acquisition equipment is kept consistent with the parameters, thereby reducing data variability. The collected images are labeled for ankle joint athletic injuries. The collected ankle joint athletic injury data information is shown in **Table 1**.

In **Table 1**, the collected data on ankle joint athletic injuries are described. In the collected ankle joint athletic injury images, there are 12 types of injuries. The characteristics exhibited by different ankle joint athletic injuries in MRI images are different, and ankle joint athletic injuries have a significant impact on the human body. The anterior cruciate ligament is an essential structure of the knee joint, mainly used to control the forward and backward movement of the knee. Injury to the anterior cruciate ligament can cause severe pain and swelling of the knee joint, reducing the patient's mobility.

Table 1. Data on ankle joint athletic injury.

Injury type	Quantity	Proportion
Anterior cruciate ligament injury	120	8.0%
Posterior cruciate ligament injury	122	8.1%
Lateral collateral ligament injury	128	8.5%
Medial collateral ligament injury	134	8.9%
Tibial fracture	135	9.0%
Fibular fracture	131	8.7%
Soft tissue injury	118	7.9%
Ankle joint bursitis	102	6.8%
Ankle joint synovial cyst	100	6.7%
Ankle joint dislocation	120	8.0%
Cartilage injury	124	8.3%
Tendinitis	166	11.1%
Total	1500	100.0%

The collected partial MRI images are shown in **Figure 2**.

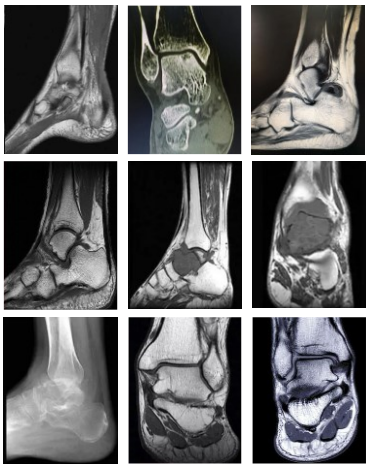

Figure 2. Partial MRI images collected.

In **Figure 2**, the collected partial MRI images are described. In order to display the structure of the ankle joint more comprehensively, MRI equipment is used to collect cross-sectional, coronal, and sagittal images of the patient's ankle joint.

2.2. Image preprocessing

After collecting enough MRI images of ankle joint athletic injury, pre-processing of the acquired image data is required in order to facilitate the subsequent accurate diagnosis of ankle joint athletic injuries. Image preprocessing is a crucial step in medical image analysis, which obtains high-quality images through preprocessing, providing reliable image data for subsequent analysis and diagnosis.

The content of image preprocessing includes image denoising, image registration, image segmentation, and data standardization processing. When using MRI equipment for image acquisition, it introduces random thermal noise, which leads to random

brightness fluctuations in the collected images and affects the diagnosis of ankle joint injuries. Moreover, both the radio frequency coil and amplifier of MRI equipment may cause noise data [25,26].

To reduce noise data in MRI images, Gaussian filtering is utilized to smooth the image and reduce high-frequency noise. The filtering kernel size of the Gaussian filter is selected as 5×5. The Gaussian filtering kernel is a two-dimensional Gaussian function, expressed as:

$$G(x,y) = ({}^{1}/_{2\pi c^2}) * e^{(-\frac{x^2+y^2}{2c^2})} \quad (1)$$

In Equation (1), (x,y) shows the position of the kernel coordinate, and $G(x,y)$ shows the value of the filtering kernel at position (x,y).

The generated Gaussian filter kernel is applied to each pixel of the MRI image. The filter kernel is multiplied by the local region of the image, and the results are added to obtain the filtered image.

$$I_1(x,y) = \sum\sum (I(a,b) * G(x-a, y-b)) \quad (2)$$

In Equation (2), $I(a,b)$ indicates the pixel value of the input image, and $G(x-a, y-b)$ indicates the value of the filtering kernel at $(x-a, y-b)$.

When performing Gaussian filtering, the zero fill method is used to process boundary pixels, thereby avoiding the filtering kernel from exceeding the boundaries of the image [27,28].

The steps of processing ankle injury MRI images include: first, denoising, reducing image noise through Gaussian filtering; then image segmentation, using thresholding to extract joint structure; then feature extraction, using edge detection to obtain key features; finally, inputting the extracted features into the selected model for classification and analysis to ensure the accuracy and reliability of the results.

Gaussian filters are often used for denoising in medical image analysis. Their advantages include effective image smoothing, reducing high-frequency noise, and retaining edge information. However, their disadvantage is that they may blur image details, especially when dealing with high-contrast areas. In addition, the degree of image smoothing by Gaussian filtering depends on the selected standard deviation, and improper parameter setting may lead to over-smoothing or under-smoothing. Despite this, Gaussian filters are still widely used in processing MRI and CT images, especially in the preprocessing step, which can improve the accuracy of subsequent analysis.

The standard deviation σ of the Gaussian filter is selected as 1.5 in order to effectively remove high-frequency noise in medical images while maintaining important details of the image. In medical image analysis, the preservation of details is crucial, especially in the diagnosis process. The filter size was chosen to be 5x5, which can avoid over-blurring the image while denoising, thus ensuring that the image still has sufficient readability and clinical value after processing.

Image registration is a key task in medical image processing. The content of different images is aligned for effective comparison, analysis, and integration. By performing operations such as translation, rotation, and scaling, the target image is

aligned to the maximum extent possible with the reference image, thereby reducing the differences between different MRI images.

The formula for translating MRI images is:

$$\begin{cases} x^{'} = x + dx \\ y^{'} = y + dy \end{cases} \tag{3}$$

In Equation (3), (x, y) is the coordinates on the original image, and $(x^{'}, y^{'})$ is the coordinates after the image is translated.

The formula for rotating MRI images is:

$$\begin{cases} x^{'} = x * \cos(b) - y * sin(b) \\ y^{'} = x * \sin(b) + y * \cos(b) \end{cases} \tag{4}$$

In Equation (4), b is the rotation angle.

The formula for scaling MRI images is:

$$\begin{cases} x^{'} = s * x \\ y^{'} = s * y \end{cases} \tag{5}$$

In Equation (5), s represents the scaling factor.

MRI image segmentation is the process of dividing different tissues or regions in an image into different parts, which facilitates the localization and recognition of specific ankle joint tissue structures. Thresholds are used to classify pixels into different regions, thereby distinguishing foreground and background information in the image.

The formula for threshold segmentation is expressed as:

$$\begin{cases} F(x,y) = 1, & I(x,y) > T \\ B(x,y) = 1, & I(x,y) \le T \end{cases} \tag{6}$$

In Equation (6), T indicates the segmentation threshold; $F(x,y)$ indicates the foreground; $B(x,y)$ represents the background.

The clarity of images collected often varies. To enhance the effectiveness of diagnosis, there is a need to standardize image data to ensure consistent brightness and contrast. The mean and standard deviation are used for linear stretching, and pixel values are remapped to specific brightness ranges:

$$P_n = (P_o - u)/d \tag{7}$$

In Equation (7), u indicates the average value of image pixels, and d indicates the standard deviation of image pixels. P_n represents the standardized pixel values, and P_o represents the pixel values of the original image.

The preprocessed findings of the MRI images are depicted in **Figure 3**.

In **Figure 3**, the findings after preprocessing are described. The image is Gaussian denoised and divided into background and foreground by setting a threshold. Image preprocessing operations can effectively denoise image noise data and divide the ankle joint region in the image into different regions, which is conducive to the diagnosis of ankle joint athletic injury.

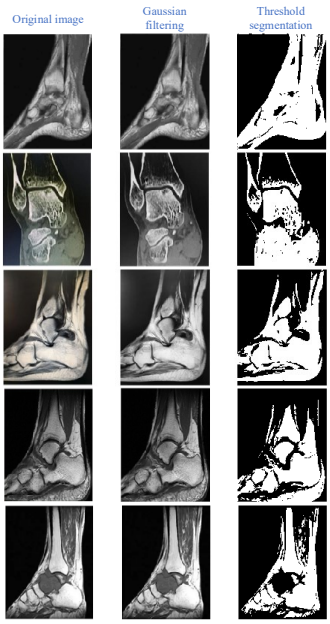

Figure 3. Results after preprocessing.

The visual changes of the image after preprocessing are shown in **Table 2**.

Table 2. Visual changes of the image after preprocessing.

Image type	PSNR (dB)	SSIM
Original image	32.5	0.87
After Gaussian filtering	35.2	0.9
After median filtering	34.8	0.89
After bilateral filtering	36.1	0.91
After histogram equalization	33.5	0.85

2.3. Feature extraction

Image feature extraction is the extraction of meaningful information or features from an image for image analysis, pattern recognition, ML, or computer vision tasks. Extracting features from the collected MRI images is beneficial for the subsequent use of ML models for ankle joint athletic injury diagnosis.

In order to comprehensively analyze the characteristics of ankle joint athletic injury, it is necessary to extract morphological and texture features from MRI images. Morphological features include joint gap width, joint cartilage morphology, etc. In the collected specific section of the ankle joint, the bone part of the ankle joint in the image is separated from the background part through threshold segmentation. The position of the bone ends is determined based on the bone edge or joint surface in the image, and the joint gap width is determined by measuring the distance between the bone ends,

After detecting the edge area of cartilage using threshold segmentation, the distance from the surface of the cartilage to the subchondral bone is measured, and the thickness of the cartilage is calculated. To ensure the accuracy of cartilage thickness measurement, the average value can be used to measure the thickness of the cartilage.

The formula for calculating the thickness of cartilage is:

$$H = \frac{\sum_{i=1}^{n}(H_i)}{n} \tag{8}$$

In Equation (8), n represents the number of times cartilage thickness is measured.

Texture features can describe the characteristics of textures and details on the surface of an image, which are formed by changes in color, brightness, or structure between adjacent pixels. By digitizing texture information, image detection and analysis can be carried out. In order to detect the type of ankle joint athletic injury based on different texture features of MRI images, local binary mode is used to extract texture feature information.

The image is converted into a grayscale image, and the local domain of the pixels is set, with a domain range of 3×3 windows. The central pixel is compared with other pixels in the surrounding area for grayscale values.

When the grayscale value of the surrounding pixels is greater than or equal to the grayscale value of the center pixel, the surrounding pixels are marked as 1. When the grayscale value of the surrounding pixels is less than the grayscale value of the center pixel, the surrounding pixels are marked as 0. The formula for converting each pixel into binary mode is represented as:

$$\begin{cases} 1, h_1 \geq h_0 \\ 0, h_1 < h_0 \end{cases} \tag{9}$$

In Equation (9), h_0 represents the grayscale value of the central pixel, and h_1 is the grayscale value of the surrounding pixels.

The 8-bit binary values in the surrounding area of the central pixel are collected and processed in a clockwise order to convert the grayscale information of the image into binary values.

To effectively enhance the accuracy of MRI image diagnosis, different image features are fused at the feature level, which is beneficial for improving the performance of data analysis and ML tasks. The formula for feature fusion is expressed as:

$$T = T_1 + T_2 \tag{10}$$

In Equation (10), T_1 represents the morphological features of the image; T_2 represents the texture features of the image; T represents the fused features.

2.4. Improved ResNet model

Residual network is a deep CNN architecture that solves the problem of gradient vanishing and gradient explosion during the training process of deep neural networks by introducing residual blocks [29,30]. In traditional CNN models, the input of each convolutional layer is processed by weights and activation functions, and then passed to the next layer. This leads to a gradual decrease in gradient after each convolutional layer, resulting in unstable or overfitting of the network model [31,32].

The ResNet model learns residual functions through residual connections. A skip connection is introduced, and the input is added to the output of the convolutional layer, forming a residual connection [33,34]. The output of the residual block is represented as:

$$F(x) = H(x) + x \tag{11}$$

In Equation (11), $H(x)$ represents the residual function.

There are still some issues with the ResNet model, and using the ReLU activation function in ResNet can help alleviate the gradient vanishing problem. However, when the ResNet model has a deeper network depth, the ReLU activation function may produce a larger gradient. Moreover, the ReLU activation function itself has certain flaws, which may lead to neuronal necrosis during neuronal training.

The traditional ResNet model uses a global average pooling layer instead of a fully connected layer, but the average pooling process is difficult to capture the most significant ankle joint athletic injury feature information [35,36]. To better analyze MRI images, the ResNet model is improved.

ResNet-50 is selected as the backbone network, and pre trained weights are used as initialization. Through transfer learning, pre trained weights are fine-tuned and feature representations from large-scale datasets are transferred to the ankle joint athletic injury diagnosis task, thereby improving model performance [37,38].

The activation function ReLU is changed to the Leaky ReLU function. By setting a small value, neurons are initialized to avoid necrosis. The expression for the Leaky ReLU function is:

$$\text{Leaky ReLU(x)} = \begin{cases} \text{x}, \text{x} > 0 \\ \text{kx}, \text{x} \leq 0 \end{cases} \tag{12}$$

In Equation (12), k is the parameter used to adjust the zero gradient problem for negative values.

The global average pooling layer averages the values of each channel in the entire feature map and outputs a scalar value, effectively reducing the number of network parameters and complexity, but it is difficult to capture the most significant features. The global average pooling layer is improved to the global maximum pooling layer. By selecting the maximum value of each channel, the feature information that best expresses ankle joint athletic injury in the image is highlighted.

The formula for the global maximum pooling layer is expressed as:

$$\text{G}_\text{r} = \text{Max}\{(\text{x}_{\text{ij}})^\text{r}\} \tag{13}$$

The improved ResNet model structure is illustrated in **Figure 4**.

In **Figure 4**, the improved ResNet model structure is described. The selected backbone network is ResNet-50, and transfer learning is used to initialize pre training weights. The activation function ReLU is modified to Leaky ReLU, and a fully connected layer is constructed through the global maximum pooling layer and softmax classifier.

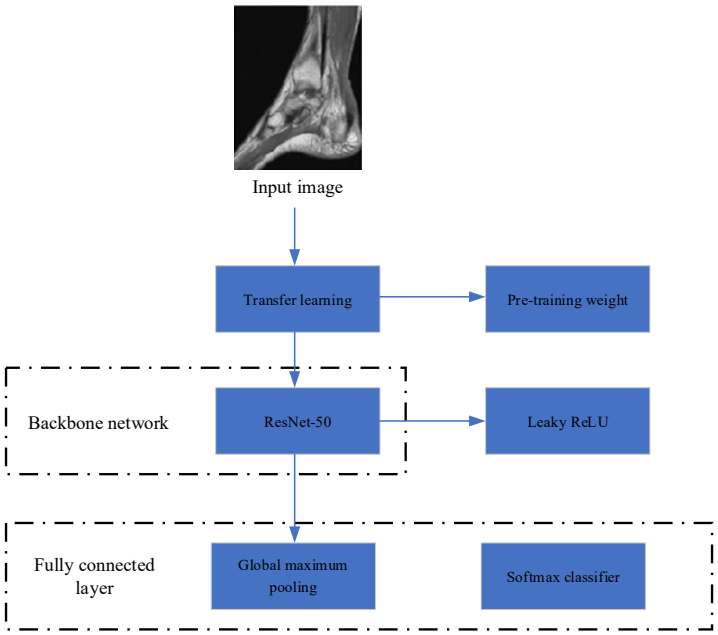

Figure 4. Improved ResNet model structure.

3. Diagnosis and evaluation of ankle joint athletic injury

3.1. Model training

The ankle joint is composed of the tibia, fibula, and talus, responsible for supporting weight, balance, and foot movement. Under intense exercise, the ankle joint is prone to injury. Using MRI equipment to scan the structure of the ankle joint is beneficial for accurate diagnosis of ankle joint injury through analysis of MRI images.

In order to effectively diagnose ankle joint athletic injury through MRI, the experiment uses an improved ResNet model for ankle joint athletic injury classification detection. The experimental environment required for training the improved ResNet model is shown in **Table 3**.

Table 3. Experimental environment required for training the improved ResNet model.

Serial number	Content	Parameter
1	MRI scanner	3T
2	Storage capacity	1TB
3	Central processing unit	Intel Core i9-11900K
4	Graphics processing unit	AMD Radeon RX 6900 XT
5	Internal storage	32GB
6	Programming language	Python
7	Programming software	PyCharm
8	Operating system	Linux
9	Deep learning framework	TensorFlow

In **Table 3**, the experimental environment required for training the improved ResNet model is described. The hardware environment and software environment required for the experiment are listed. The Python language is used to construct improved ResNet models by introducing the TensorFlow framework.

In order to effectively train and test the improved ResNet model, the collected MRI image dataset is divided into bit training and testing sets. The results of dividing the dataset using 5-fold cross validation are displayed in **Table 4**.

Table 4. Results of dataset partitioning.

Injury type	Test set	Training set
Anterior cruciate ligament injury	24	96
Posterior cruciate ligament injury	24	98
Lateral collateral ligament injury	26	102
Medial collateral ligament injury	27	107
Tibial fracture	27	108
Fibular fracture	26	105
Soft tissue injury	24	94
Ankle joint bursitis	20	82
Ankle joint synovial cyst	20	80
Ankle joint dislocation	24	96
Cartilage injury	25	99
Tendinitis	33	133
Total	300	1200

In **Table 4**, the results of dataset partitioning are described. The 5-fold cross validation divides the entire dataset into 5 subsets, selecting one subset as the test set and the other 4 subsets as the training set, and iterating 5 times. The content of the test set is changed every time until all data is trained and tested. The use of 5-fold cross validation to partition the dataset can fully utilize image sample data. There are 300 images in total for the test set and 1200 images in total for the training set.

In the improved ResNet model constructed, the batch size is set to 32 and the number of iterations is 100. The cross entropy loss function is used as the loss function of the Softmax classifier, and the learning rate of the improved ResNet model is set to 0.0001.

The pre trained weights are used to initialize the model, and the training data is input into the network model for training. By using the cross entropy loss function, the output of the model is compared with the real label, and the difference between the output content and the real label is calculated. The calculated loss value is propagated through feedback, and the weights of the stochastic gradient descent optimization network model are used to minimize the loss function.

The model parameters are set with a batch size of 32 and a training round of 50. The Adam optimizer is used to accelerate convergence. The loss function uses cross entropy to evaluate the classification effect. During the training process, the data set is divided into a training set (80%) and a validation set (20%), and an early stopping strategy is used to prevent overfitting. After each round of training, the model

performance is evaluated through the validation set and the best model parameters are recorded. The model gradually adjusts the hyperparameters to ultimately achieve the optimal damage identification effect.

The hyperparameter comparison results of different algorithms are shown in **Table 5**.

Table 5. Hyperparameter comparison results of different algorithms.

Model	Learning rate	Batch size	Iterations	Optimization Algorithm	Hyperparameters
Improved ResNet	0.001	32	100	Adam	N/A
ResNet-50	0.001	64	200	SGD	N/A
Inception	0.0001	32	150	Adam	N/A
SVM	N/A	N/A	N/A	Use default settings	C=1, kernel=RBF, gamma=0.1
RF	N/A	N/A	N/A	Use default settings	n_estimators=100, max_depth=10

3.2. Evaluation indicators

After sufficient training of the improved ResNet model, the performance of the improved ResNet model for ankle joint athletic injury classification is analyzed using data from the test set for validation. The internal structure of the ankle joint is complex, and the types of ankle joint athletic injuries are determined by the injuries in different parts and the degree of injury.

From MRI images, the findings of ankle joint athletic injury are analyzed and can be compared with actual labels through image classification. TP indicates that ankle joint athletic injuries are classified as positive cases and the actual cases are also positive cases; FP indicates that ankle joint athletic injuries are classified as positive cases but actually as negative cases; FN indicates that ankle joint athletic injuries are classified as negative cases but are actually positive cases; TN indicates that ankle joint athletic injuries are classified as negative cases and are actually also negative cases.

According to the classification findings and the actual label combination, the accuracy, precision, recall, and F1 value of ankle joint athletic injury classification can be calculated. When evaluating the performance of a classification model, it is crucial to choose accuracy, precision, recall, and F1 score. Accuracy reflects the correctness of the overall classification, while precision measures the reliability of the positive class prediction. Recall indicates the model's ability to identify the positive class. The F1 score combines precision and recall, and is suitable for unbalanced data sets, ensuring that the risks of misclassification and missed classification are taken into account when optimizing the model.

The accuracy of ankle joint athletic injury classification is expressed by the formula:

$$\text{Accuracy} = {(\text{TP} + \text{TN})}\Big/{(\text{FP} + \text{TP} + \text{FN} + \text{TN})} \tag{14}$$

The precision rate of ankle joint athletic injury classification is expressed by the formula:

$$\text{Precision} = {}^{\text{TP}}\!/_{(\text{TP} + \text{FP})} \tag{15}$$

The recall rate of ankle joint athletic injury classification is expressed by the formula:

$$\text{Recall} = {}^{\text{TP}}\!/_{(\text{TP} + \text{FN})} \tag{16}$$

The F1 value is calculated by combining precision and recall, and the formula for F1 value is:

$$\text{F1} = {}^{2(\text{Pricision} \times \text{Recall})}\!/_{(\text{Pricision} + \text{Recall})} \tag{17}$$

To test and improve the stability of the ResNet model, a previous example of cruciate ligament injury is tested. The test samples of anterior cruciate ligament injury are mixed with other types of ankle joint athletic injury test samples in sequence. The stability of the improved ResNet model for ankle joint athletic injury classification is observed under different test sample conditions.

To comprehensively compare the performance of the improved ResNet model in diagnosing ankle joint athletic injuries, the improved ResNet model is compared with ResNet-50, Inception, SVM, and RF models to compare the classification performance of different models for ankle joint athletic injuries. In order to visually observe the effectiveness of different models in classifying ankle joint injuries, the classification results of different models are plotted into receiver operating characteristic (ROC) curves. The performance of the improved ResNet model in classifying ankle joint injuries is evaluated based on the characteristics of the ROC curves.

4. Results

4.1. Accuracy and precision of injury classification

There are various types of ankle joint athletic injuries, including anterior cruciate ligament injury, posterior cruciate ligament injury, lateral collateral ligament injury, medial collateral ligament injury, tibial fracture, fibular fracture, soft tissue injury, ankle joint bursitis, ankle joint synovial cyst, ankle joint dislocation, cartilage injury, and tendinitis, which are respectively recorded as A, B, C, D, E, F, G, H, I, J, K, and L. According to the ResNet model, improvements were made to enhance the accuracy and precision of the ResNet model for classifying ankle joint athletic injuries, as illustrated in **Figure 5**.

In **Figure 5**, the accuracy and precision of the improved ResNet model for classifying ankle joint athletic injuries are described. The horizontal axis represents 12 types of ankle joint athletic injuries, while the vertical axis represents values of accuracy and precision. The classification accuracy and precision of the improved ResNet model varied among different types of ankle joint athletic injuries, mainly due to the different characteristics of different types of ankle joint athletic injuries, the difficulty of classification recognition, and the effectiveness of model training. The improved ResNet model had high accuracy and precision in classifying different types of injuries, with all values greater than 96.0%. The average classification accuracy of the improved ResNet model in different ankle joint athletic injuries was 98.3%, and

the average classification precision was 97.1%. The improved ResNet model can effectively classify ankle joint athletic injuries in MRI images accurately.

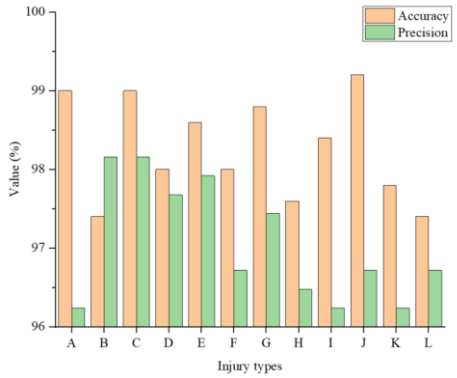

Figure 5. Accuracy and precision of injury classification.

4.2. Recall rate and F1 value for injury classification

To evaluate the performance of the improved ResNet model for diagnosing ankle joint athletic injuries from multiple perspectives, the recall and F1 value of the improved ResNet model for classifying ankle joint athletic injuries are illustrated in **Figure 6**.

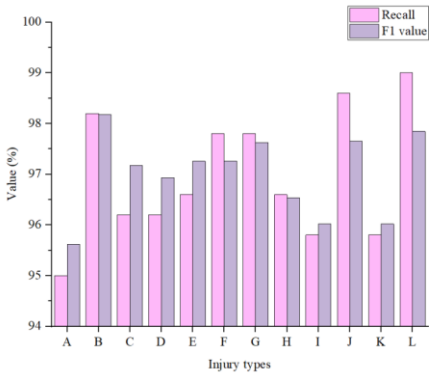

Figure 6. Recall rate and F1 value for injury classification.

In **Figure 6**, the recall rate and F1 value of the improved ResNet model for ankle joint athletic injury classification are described. The horizontal axis is the type of ankle joint athletic injury. The global maximum pooling layer and softmax classifier were used instead of the fully connected layer. By retaining the most significant features in each channel and ignoring irrelevant information, ankle joint athletic injury classification was achieved. The recall rate and F1 value of the improved ResNet model for ankle joint athletic injury classification were both high, indicating that the model can capture the majority of ankle joint athletic injury situations with good precision. The average classification recall rate of the improved ResNet model in different ankle joint athletic injuries was 97.0%, and the average classification F1 value was 97.0%. In a large number of MRI images, the improved ResNet model was used for ankle joint athletic injury classification, with excellent classification recall and F1 value. The improved ResNet model can accurately diagnose ankle joint athletic injuries in MRI images.

4.3. Confusion matrix

There are many types of ankle joint athletic injuries. The classification results of specific injury types using the improved ResNet model in the test set are shown in **Figure 7**.

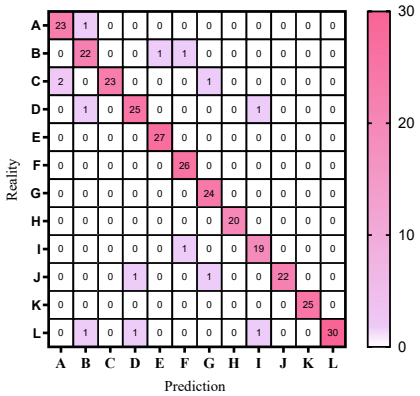

Figure 7. Confusion matrix.

In **Figure 7**, the confusion matrix for improving the ResNet model to classify specific ankle joint injuries is described. The sample size in the test set was 300, and the elements on the diagonal line connecting the upper left and lower right corners were the actual categories that were the same as those predicted by the classification. 286 samples were correctly classified for ankle joint athletic injuries. The total number of test samples for anterior cruciate ligament injury was 24, of which 23 samples were correctly classified and 1 sample was incorrectly classified as posterior cruciate ligament injury. The total number of test samples for posterior cruciate ligament injury was 24, with 22 samples correctly classified, but two samples incorrectly classified as tibial and fibular fractures. Therefore, the application of the improved ResNet model can accurately classify specific types of ankle joint injuries and achieve accurate MRI diagnosis.

4.4. Improving the stability of ResNet model

The stability results of the improved ResNet model in different test sample environments are illustrated in **Figure 8**.

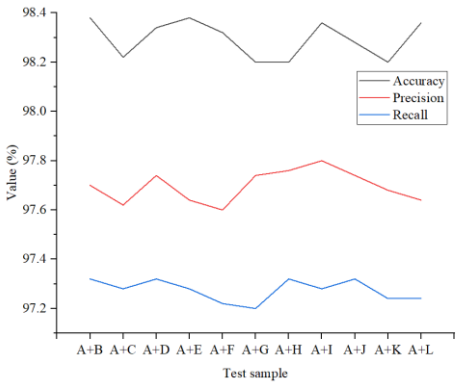

Figure 8. Stability results.

In **Figure 8**, the stability results of the improved ResNet model under different test sample environments are described. The horizontal axis represents the mixing of anterior cruciate ligament injury samples with other types of injury samples. In a mixed sample environment of 11 groups, the accuracy, precision, and recall rate values may fluctuate, but the overall fluctuation was not significant. The numerical fluctuations of accuracy, precision, and recall rate were all within 0.2%. Therefore, improving the ResNet model for ankle joint athletic injury classification had high stability.

4.5. Injury classification performance of different models

Improved ResNet, ResNet-50, Inception, SVM, and RF models were compared. The accuracy of ankle joint injury classification for different models is shown in **Table 6**.

Table 6. Accuracy of ankle joint injury classification by different models.

Injury types	Improved ResNet (%)	ResNet-50 (%)	Inception (%)	SVM (%)	RF (%)
A	99.0	96.4	92.8	80.0	82.9
B	97.4	95.5	92.8	80.0	83.5
C	99.0	95.2	95.6	84.2	82.0
D	98.0	95.2	92.4	81.8	83.2
E	98.6	94.3	93.2	81.8	82.0
F	98.0	96.4	95.2	81.8	82.6
G	98.8	94.6	95.2	83.6	84.7
H	97.6	95.5	93.2	80.0	84.1
I	98.4	96.4	94.8	86.0	85.0
J	99.2	96.1	94.4	80.0	83.2
K	97.8	94.0	95.2	83.6	83.8
L	97.4	96.4	92.8	80.0	82.9

In **Table 6**, the accuracy of ankle joint injury classification for different models is described. Five models were compared and analyzed. The accuracy of the improved ResNet model in classifying ankle joint injuries was higher than that of the other four models. This is mainly due to the improved ResNet model using the Leaky ReLU activation function to avoid neuronal necrosis, and the utilization of a global maximum pooling layer to capture the most significant ankle joint injury features. The accuracy of improving ResNet, ResNet-50, Inception, SVM, and RF models for anterior cruciate ligament injury classification was 99.0%, 96.4%, 92.8%, 80.0%, and 82.9%, respectively. The AUC values of Improved ResNet, ResNet-50, Inception, SVM, and RF are 0.92, 0.90, 0.89, 0.86, and 0.85, respectively.

4.6. Results of ROC curve

The comparison of ROC curves of different models is illustrated in **Figure 9**.

In **Figure 9**, the ROC curves of different models are compared. The ROC curve represented by the improved ResNet model was at the top and the area enclosed below was the largest, indicating that the improved ResNet model had the highest precision

in classifying ankle joint athletic injuries. By improving the ResNet model, the precision of ankle joint athletic injury classification can be effectively improved.

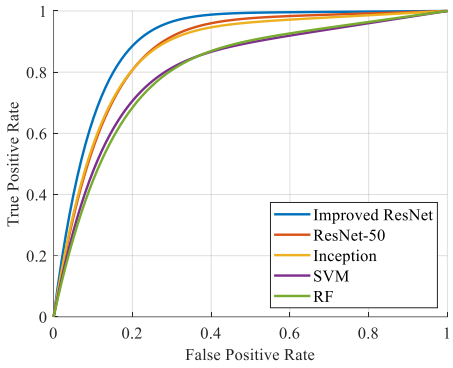

Figure 9. Comparison of ROC curves.

5. Conclusions

As medical imaging technology rapidly advances, the use of MRI can display the complete ankle joint injury area, helping doctors accurately diagnose and assess the severity of the injury. The ResNet model was improved and the activation function was replaced. Transfer learning was used to initialize the model, and through the global maximum pooling layer, the fully connected layer was constructed. The outcomes showed that the improved ResNet model can accurately classify different types of ankle joint athletic injuries and maintain high stability in different sample environments. Applying the improved ResNet model to MRI diagnosis helps doctors improve the effectiveness of ankle joint injury diagnosis by accurately classifying and analyzing ankle joint athletic injuries, thereby enabling doctors to more accurately understand the nature and severity of injuries. However, the number of MRI images collected in this article is not enough. Collecting more types of ankle joint athletic injury MRI images and conducting injury classification analysis would be the direction of future research. Collecting more types of ankle injury MRI images is crucial to improving the generalization ability of the model. This will enhance the model's ability to identify different types of injuries, improve the accuracy of diagnosis, help develop more effective treatment plans, and ultimately improve the patient's recovery.

Author contributions: Conceptualization, HH and YL; methodology, HH; software, HH; validation, YL; formal analysis, HH; investigation, YL; resources, HH; data curation, HH; writing—original draft preparation, HH; writing—review and editing, YL; visualization, HH; supervision, HH; project administration, YL; funding acquisition, HH. All authors have read and agreed to the published version of the manuscript.

Ethical approval: Not applicable.

Conflict of interest: The authors declare no conflict of interest.

References

1. Herzog, Mackenzie M., Zachary Y. Kerr, Stephen W. Marshall, Erik A. Wikstrom. "Epidemiology of ankle sprains and chronic ankle instability." Journal of athletic training 54.6 (2019): 603-610, DOI: https://doi.org/10.4085/1062-6050-447-17.
2. Vosseller, J. Turner, Elizabeth R. Dennis, and Shaw Bronner. "Ankle injuries in dancers." JAAOS-Journal of the American Academy of Orthopaedic Surgeons 27.16 (2019): 582-589, DOI: 10.5435/JAAOS-D-18-00596.
3. Stupic, Karl F., Maureen Ainslie, Michael A. Boss, Cecil Charles, Andrew M. Dienstfrey, Jeffrey L. Evelhoch, et al. "A standard system phantom for magnetic resonance imaging." Magnetic resonance in medicine 86.3 (2021): 1194-1211, DOI: https://doi.org/10.1002/mrm.28779.
4. Knoll, Florian, Kerstin Hammernik, Chi Zhang, Steen Moeller, Thomas Pock, Daniel K. Sodickson, et al. "Deep-learning methods for parallel magnetic resonance imaging reconstruction: A survey of the current approaches, trends, and issues." IEEE signal processing magazine 37.1 (2020): 128-140, DOI: 10.1109/MSP.2019.2950640.
5. Sun Yulong. "CT image post-processing combined with magnetic resonance technology for the classification, diagnosis, and prognosis analysis of ankle joint fracture patients." Heilongjiang Medical Journal 45.17 (2021): 1869-1870.
6. Chen Jian. "Comparative study of multi row spiral CT combined with MRI in the diagnosis of lateral ligament injury of the ankle joint." Chinese Medical Equipment 34.3 (2019): 64-67.
7. Zhang Qianying, Liu Xuhong, Huang Ying, Han Xiaobing, Zhang Sizhu, A Huan, et al. "The effect of magnetic resonance three-dimensional water excitation sequence on ankle joint cartilage imaging." Journal of Molecular Imaging 45.4 (2022): 572-575.
8. Ye Yunkai. "Analysis of the Clinical Significance of High Field Magnetic Resonance (MR) Diagnosis of Ankle Joint Anterolateral Impact Syndrome." Chinese Medical Device Information 24.23 (2018): 41-43.
9. Gorbachova, Tetyana. "Magnetic resonance imaging of the ankle and foot." Polish Journal of Radiology 85.1 (2020): 532-549, DOI: https://doi.org/10.5114/pjr.2020.99472.
10. Alves, Timothy, Qian Dong, Jon Jacobson, Corrie Yablon, Girish Gandikota. "Normal and injured ankle ligaments on ultrasonography with magnetic resonance imaging correlation." Journal of Ultrasound in Medicine 38.2 (2019): 513-528, DOI: https://doi.org/10.1002/jum.14716.
11. Sawant, Yogini Nilkantha, and Darshana Sanghvi. "Magnetic resonance imaging of ankle ligaments: A pictorial essay." Indian Journal of Radiology and Imaging 28.04 (2018): 419-426, DOI: 10.4103/ijri.IJRI_77_16.
12. Warner, Stephen J., Matthew R. Garner, Dean G. Lorich. "The diagnostic accuracy of radiographs and magnetic resonance imaging in predicting deltoid ligament ruptures in ankle fractures." HSS Journal® 15.2 (2019): 115-121, DOI: https://doi.org/10.1007/s11420-018-09655-x.
13. Pan Yaling, Wang Hanqi, and Lu Yong. "The Application of Artificial Intelligence in Medical Imaging CAD." International Journal of Medical Radiology 42.1 (2019): 3-7.
14. Liu Wenguang, Xie Simin, Zhou Yafang, Hu Jiaxi, Li Mengsi, Li Wenzheng, et al. "Machine learning and its research progress in imaging diagnosis of liver diseases." International Journal of Medical Radiology 42.1 (2019): 16-21.
15. Giger, Maryellen L. "Machine learning in medical imaging." Journal of the American College of Radiology 15.3 (2018): 512-520, DOI: https://doi.org/10.1016/j.jacr.2017.12.028.
16. Rana, Meghavi, and Megha Bhushan. "Machine learning and deep learning approach for medical image analysis: diagnosis to detection." Multimedia Tools and Applications 82.17 (2023): 26731-26769.
17. Willemink, Martin J., Wojciech A. Koszek, Cailin Hardell, Jie Wu, Dominik Fleischmann, Hugh Harvey, et al. "Preparing medical imaging data for machine learning." Radiology 295.1 (2020): 4-15, DOI: https://doi.org/10.1148/radiol.2020192224.
18. Yadav, Samir S., and Shivajirao M. Jadhav. "Deep convolutional neural network based medical image classification for disease diagnosis." Journal of Big data 6.1 (2019): 1-18.
19. Sarvamangala, D. R., and Raghavendra V. Kulkarni. "Convolutional neural networks in medical image understanding: a survey." Evolutionary intelligence 15.1 (2022): 1-22.
20. Poedjiastoeti, Wiwiek, and Siriwan Suebnukarn. "Application of convolutional neural network in the diagnosis of jaw tumors." Healthcare informatics research 24.3 (2018): 236-241, DOI: https://doi.org/10.4258/hir.2018.24.3.236.
21. Chen Mingliang, Gu Chengyi, Xu Liuhai, Zhou You. "Research progress in the diagnosis and treatment of lateral collateral ligament injury in the ankle joint." Chinese Journal of Sports Medicine 38.2 (2019): 152-158.

22. Chen Xin, Shi Shaoyun, Chen Xiuqing, Hu Baijun, Chen Shurong. "The application of exercise therapy in the rehabilitation treatment of ankle joint injuries." Chinese Journal of Bone and Joint Injury 33.8 (2018): 892-893.
23. Gulbrandsen, Matthew, David E. Hartigan, Karan A. Patel, Justin L Makovicka, Sailesh V Tummala, Anikar Chhabra, et al. "Ten-year epidemiology of ankle injuries in men's and women's collegiate soccer players." Journal of athletic training 54.8 (2019): 881-888, DOI: https://doi.org/10.4085/1062-6050-144-18.
24. Skazalski, Christopher, Jacek Kruczynski, Martin Aase Bahr, Tone Bere, Rod Whiteley, Roald Bahr, et al. "Landing-related ankle injuries do not occur in plantarflexion as once thought: a systematic video analysis of ankle injuries in world-class volleyball." British journal of sports medicine 52.2 (2018): 74-82, DOI: http://dx.doi.org/10.1136/bjsports-2016-097155.
25. Drost, Frank-Jan H., Daniel Osses, Daan Nieboer, Chris H. Bangma, Ewout W. Steyerberg, Monique J. Roobol, et al. "Prostate magnetic resonance imaging, with or without magnetic resonance imaging-targeted biopsy, and systematic biopsy for detecting prostate cancer: a Cochrane systematic review and meta-analysis." European urology 77.1 (2020): 78-94, DOI: https://doi.org/10.1016/j.eururo.2019.06.023.
26. Keenan, Kathryn E., Maureen Ainslie, Alex J. Barker, Michael A. Boss, Kim M. Cecil, Cecil Charles, et al. "Quantitative magnetic resonance imaging phantoms: a review and the need for a system phantom." Magnetic resonance in medicine 79.1 (2018): 48-61, DOI: https://doi.org/10.1002/mrm.26982.
27. Zhao, Kai, Li-Guo Tan, and Shen-Min Song. "Gaussian filter for nonlinear networked systems with synchronously correlated noises and one-step randomly delayed measurements and multiple packet dropouts." IEEE Sensors Journal 19.20 (2019): 9271-9281.
28. Li Jian, Ding Xiaoqi, Chen Guang, Sun Yang, Jiang Nan. "A denoising method for leaf images based on improved Gaussian filtering algorithm." Southern Agricultural Journal 50.6 (2019): 1385-1391.
29. Boroumand, Mehdi, Mo Chen, and Jessica Fridrich. "Deep residual network for steganalysis of digital images." IEEE Transactions on Information Forensics and Security 14.5 (2018): 1181-1193.
30. Wang, Ruhua, Wanquan Liu. "Deep residual network framework for structural health monitoring." Structural Health Monitoring 20.4 (2021): 1443-1461, DOI: https://doi.org/10.1177/1475921720918378.
31. Dhillon, Anamika, and Gyanendra K. Verma. "Convolutional neural network: a review of models, methodologies and applications to object detection." Progress in Artificial Intelligence 9.2 (2020): 85-112.
32. Cong, Iris, Soonwon Choi, and Mikhail D. Lukin. "Quantum convolutional neural networks." Nature Physics 15.12 (2019): 1273-1278.
33. Wang Ke, and Zhang Genyao. "Thyroid SPECT imaging diagnosis based on ResNet model." Journal of Hebei University of Science and Technology 41.3 (2020): 242-248.
34. Zheng Yao, Zhang Ye, Du Peng, Zhang Wenli, Liu Yang, Zhang Xi, et al. "Research on the application of ResNet model construction based on T2W magnetic resonance imaging in the double objective prediction of bladder cancer grading and staging." China Medical Equipment 17.8 (2020): 1-4.
35. Zheng Qiumei, Tan Dan, and Wang Fenghua. "Research on Traffic Sign Recognition Based on Improved ResNet Networks." Computer and Digital Engineering 49.5 (2021): 947-951.
36. Jin Ying, Ye Sa, and Li Honglei. "Research on an Intelligent Diagnosis Model for Fruit Tree Diseases Based on ResNet-50 Deep Convolutional Network." Journal of Agricultural Library and Information Science 33.4 (2021): 58-67.
37. Maican, C. I., Sumedrea, S., Tecau, A., Nichifor, E., Chitu, I. B., Lixandroiu, R., & Bratucu, G. (2023). Factors Influencing the Behavioural Intention to Use AI-Generated Images in Business: A UTAUT2 Perspective with Moderators. Journal of Organizational and End User Computing, 35(1), 1-32.
38. Wu, J., & Zhang, K. (2022). Machine Learning Algorithms for Big Data Applications with Policy Implementation. Journal of Organizational and End User Computing, 34(3), 1-13.